Synthesis of Single Phase Tin(II) Oxide Nanoparticles by Microwave-Assisted Hydrothermal Technique

Manouchehri, Sohrab*[+]; Boroojerdian, Parviz; Marasi, Atefe; Amoo, Maryam; Yousefi, Mohammad Hassan

Department of Physics, Malek-Ashtar University of Technology, Shahinshahr, Isfahan, I.R. IRAN

ABSTRACT: *This paper presents a novel microwave-assisted hydrothermal technique for synthesizing tin(II) oxide nanoparticles. This technique can be used for producing large quantities of homogeneous nanoparticles in a short time. The effect of the solution molarity, final pH, hydrothermal processing time and microwave power were studied. The tin(II) oxide structure verified from XRD and the mean crystallite size was evaluated to be about 5 nm using the Debye-Scherrer formula on the most intense peak. The particle size was measured from STM pictures in the range between 4-5 nm. For different samples, UV-Vis spectroscopy showed the absorption peak due to tin(II) oxide at about 240 nm and an exitonian peak at about 280 nm that shifted with respect to solution molarity, final pH, hydrothermal processing time and microwave power. The photoluminescence spectroscopy (PL) results showed the emission peaks in the visible spectrum range. The results showed that synthesized SnO nanoparticles have a direct band gap equal to about 2.5 eV, an Urbach energy of about 2.7 eV and activation energy of 47.75 kJ/mol.*

KEYWORDS: *Tin(II) oxide nanoparticles; Microwave-assisted hydrothermal technique; Urbach energy; Activation energy*.

INTRODUCTION

Since the middle of 20th century, semiconductors have been playing an imprtant role in the electronic industries[1]. In today's world, the research for synthesizing new semiconductors or improving existing materials has been expanded [2].

Oxide semiconductors have different kinds of crystal structures which lead to different electronic and optical properties [3]. They have many advantages compared to non-oxide semiconductors, such as wide band coverage suitable for applications with short wavelength light, transparency and simple coloring with pigments, high n-type carrier concentrations, the capability to be grown at low temperatures even on plastic substrates, ecological safety and low cost [4].

There are two types of tin oxides, tin(II) oxide and tin(IV) oxide, both of which have semiconducting properties. Tin(IV) oxide is more stable, so it can be synthesized easier. As a result, it is used more often and its properties are more thoroughly researched [5]. Tin(II) oxide is less stable so there is too little information about it.

Nanoparticles of oxide semiconductors have been synthesized by various methods and techniques such as

* *To whom correspondence should be addressed.*
+ *E-mail: dez283@yahoo.com*
1021-9986/2018/6/1-8 *8/$/5.08*

hydrotermal, microwave techniques, CVD, sputtering, sonochemical and mechanochemical [6]. For the synthesis of SnO nanostructure, different methods have been reported, such as hydrothermal [7], sonochemical [8], combustion [9], co-precipitation [6], gas phase condensation [10], ionthermal [11] and sputtering [12]. In most of these methods, the final products are multi-phase with structures of nanowhiskers, flowerlike, nanodiskettes, nano plates, nano robs, etc [7-12].

The goal of this research is the synthesis of single phase tin(II) oxide nanoparticles by hydrotermal microwave-assisted technique. This new technique is cheaper, more reachable and has higher efficiency in comparison with the existing techniques, because of simple equipment used in the synthesis process and short-time experimental processes. In addition, there arefewer limitations on the number of synthesized products.

EXPERIMENTAL SECTION

Sample synthesis

The preliminary materials were Sn (Alfa-Aesar 99.99%), NH_4OH (Merck 25%) and HCl (Merck 37%). First, Sn was dissolved in deionized water and an HCl solution which yields a homogeneous 0.05M solution. Then, HCl was added to the solution under stirring at room temperature to decrease the pH. Next, an aqueous ammonia solution was introduced drop wise into the solution until reaching the final pH (Table 1). Finally, microwave–assisted hydrothermal treatment was performed using a Panasonic NN-St870W type of instrument for given hydrothermal processing time and at a microwave power 300 W (Table 1). The precipitate was centrifuged and washed many times with water and allowed to dry at room temperature. The other samples were synthesized in a similar way, with different solution molarity, final pH, hydrothermal processing time and microwave power. The color of the samples was creamy white. Table 1 shows the sample codes and synthesis conditions.

Instrumental analysis

The sample characterization was done using X-ray diffraction (XRD- X'Pert Pro MPD- PANalytical), STM (SS3-Pars Nano system), UV-Vis and photoluminescence spectroscopy (PL) (T70 UV-Vis Spectrometer PG Instruments Ltd). The mean crystallite size was evaluated from the most intense peak of XRD using the Debye-Scherrer formula:

$$D = 0.9\lambda/\beta\cos\theta \quad (1)$$

Where λ is the X-ray wavelength (1.5406Å), β is the Full Width at Half Maximum (FWHM) and θ is the Bragg's diffraction angle [13]. The morphology and size of nanoparticles were characterized by Scanning Tunneling Microscopy (STM).

The optical properties of as-synthesized samples were studied at room temperature by using PL and UV-Vis spectrum. By studying the UV-Vis spectrum, the band gap energy and particle size were estimated. Equation 2 is the relation between absorption wavelength and band gap energy:

$$E_g = h\nu = hc/\lambda = 1240\left(eV.nm\right)/\lambda_{max}\left(nm\right) \quad (2)$$

Where *h* is Planck's constant, *v* is the frequency, *c* is the speed of light and λ_{max} is the excitonian peak wavelength. The particle size was calculated from the Brass equation:

$$E_g = E_g^{nano} - E_g^{bulk} = \frac{\hbar^2\pi^2}{2MR^2} \quad (3)$$

Where $\hbar$ is the reduced Plank constant, *R* is the radius of nanoparticles and *M* is the reduced mass of exciton [14].

The type of optical band gap of synthesized samples can be determined using absorption coefficient (α), the band gap and the following relation:

$$\left(\alpha h\nu\right) = B\left(h\nu - E_g\right)^m \quad (4)$$

Where E_g is the band gap, $h\nu$ is the incident photon energy, *B* is a factor depending on the transition probability and m is an integer which depends on the type of electron transition (direct or indirect). Equation (4) can be written as follows:

$$Ln\left(\alpha h\nu\right) = Ln\left(B\right) + mLn\left(h\nu - E_g\right) \quad (5)$$

The slope of diagram Ln (αhν) with respect to Ln (hν-Eg) will show the parameter m. If m is equal to 0.5, the band gap is direct [15]. Usually, there is an area in the absorption spectrum in which the absorbance increases with frequency exponentially according to the following equation:

Table 1: Solution molarity, final pH, hydrothermal processing time and microwave power of prepared samples.

Sample code	solution molarity (M) (±0.001)	Final pH (±0.01)	hydrothermal processing time (s) (±1)	Microwave power (W)
B0M3-1	0.050	1.00	0	300
B4M3-1	0.050	1.00	440	300
B7M3-1	0.050	1.00	770	300
B12M3-1	0.050	1.00	1320	300
B17M3-1	0.050	1.00	1870	300
B22M3-1	0.050	1.00	2420	300
B32M3-1	0.050	1.00	3520	300
B32M3-2.5	0.050	2.50	3520	300
B32M3-3.5	0.050	3.50	3520	300
B32M3-9	0.050	9.00	3520	300
B32M3-2	0.050	2.00	3520	300
B32L3-2	0.010	2.00	3520	300
B32H3-2	0.100	2.00	3520	300
B22M5-1	0.050	1.00	2420	500
B22M9-1	0.050	1.00	2420	900

$$\alpha = A\exp\left(\hbar\omega/E_u\right) \quad (6)$$

Where ħω is photon energy and E_u is the Urbach energy. Actually, the Urbach energy is obtained by diagram Lnα with respect to ħω [16]. The activation energy is the minimum energy that is needed for starting a chemical reaction. Arrhenius has expressed the relation between the rate of a reaction (K), temperature (T) and activation energy (E) as the following equation [17]:

$$K = A\exp\left(-E/RT\right) \quad (7)$$

Where *R* is universal gas constant. This equation can be written as follows:

$$LnK = -E/RT + LnA \quad (8)$$

E will be obtained by the slope of Ln K with respect to T^{-1}. The activation energy is related to the particle size with the following equation:

$$LE = -RT\,Ln\left(d/a\right) \quad (9)$$

Where *T* is the solution temperature, *d* is the particle size and a is a constant [18]. *Bengu et al.* used Equation (9) that is extracted from the Arrhenius equation, to calculate the activation energy.

RESULTS AND DISCUSSION

Fig. 1 shows a typical X-ray diffraction pattern for the sample B32M3-1. All the diffraction peaks of XRD pattern are matched by JCPDS card number 00-007-0195 that represents the single phase structure of SnO that well indexed to the tetragonal rutile structure with a lattice constant of a=b= 3.807 Å and c=3.834 Å. The mean crystallite size of the synthesized material was calculated by Equation (1) to be about 5 nm.

Fig. 2 represents a typical STM image of the prepared samples. This figure shows clearly that SnO nanoparticles are in the range of 4-5 nm and uniform in size.

The optical absorbance of the synthesized SnO nanoparticles for different hydrothermal processing time, which was characterized by UV-Vis absorption, is shown in Fig. 3. It can be seen that without any hydrothermal process, there is a peak in a wavelength of 240 nm. This peak is not shifted at any time of the hydrothermal process by changing pH, molarity, etc. There is also another peak in wavelength of about 280 nm in other samples, which

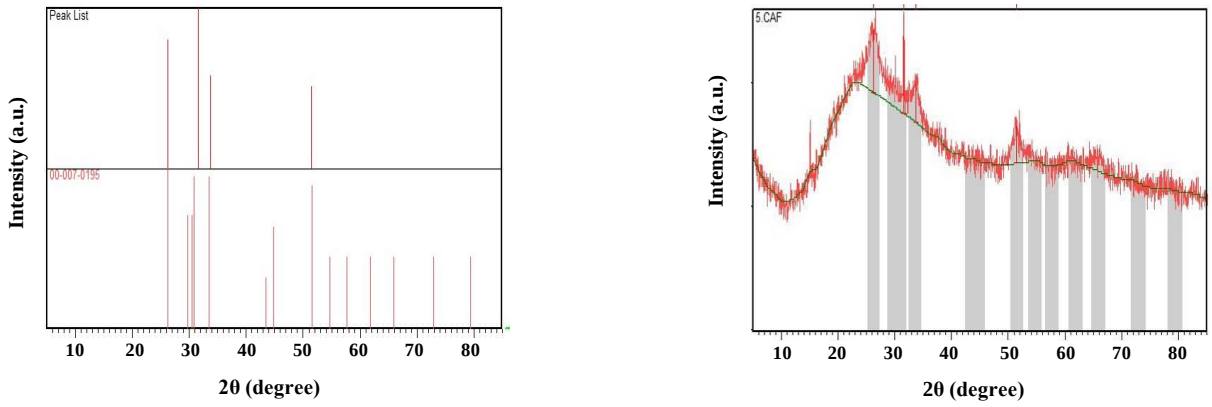

Fig. 1: X-ray diffraction pattern of sample B32M3-1, JCPDS card number 00-007-0195 and sample peaks list.

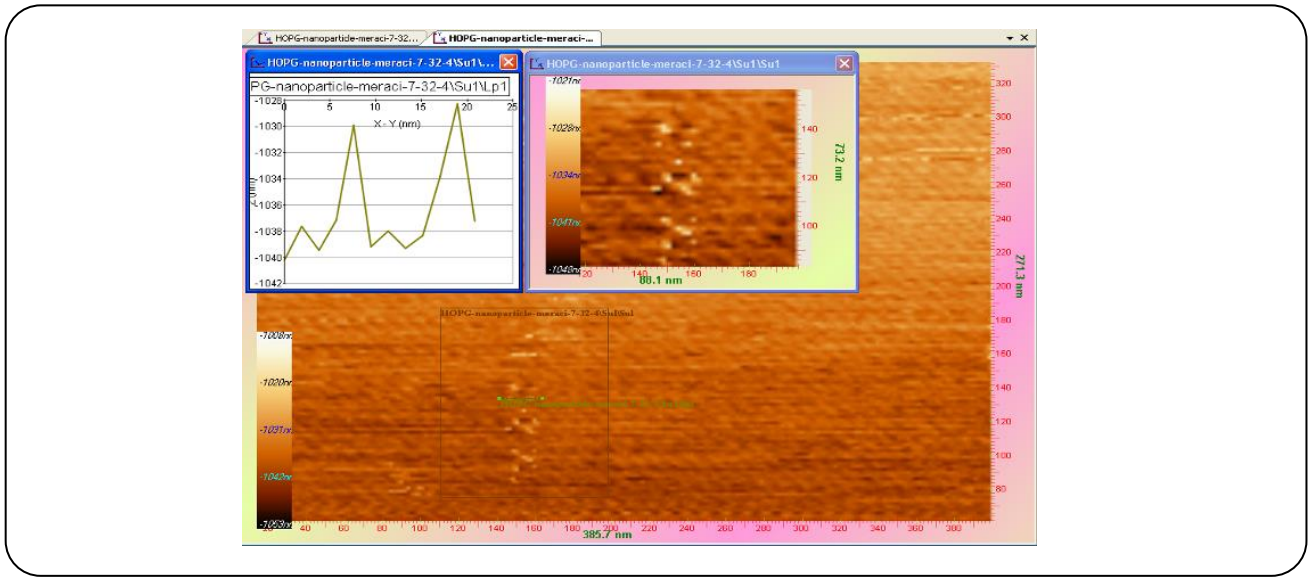

Fig. 2: STM image of B32M3-1.

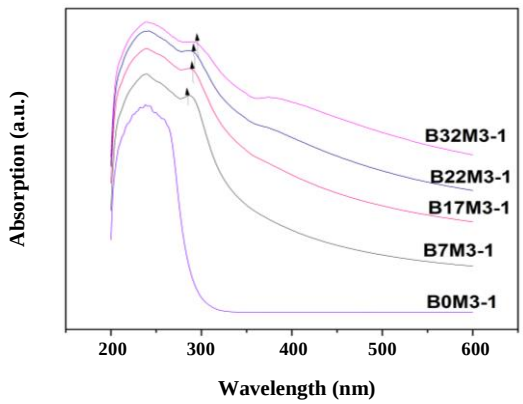

Fig. 3: UV-Vis absorption spectrum of the synthesized SnO nanoparticles.

Is considered as absorption edge. As shown in Fig. 3, the optical absorption edge shifts to higher wavelengths (red shift) as the hydrothermal process time increases, which indicates that SnO nanoparticles become larger by increasing time of hydrothermal processing.

The band gap energy and particle size were calculated from Equations (2) and (3). The results of band gap energy, absorption wavelength, and particle size are listed in Table 2. The band gap energy decreases with increasing time of hydrothermal process due to an increase in nanoparticle size.

It seems that the mechanism of SnO nanoparticles formation process is the following: At the beginning, OH^- is connected to Sn ion. Then, by increasing these connections, a cloudy net of clusters will appear. Finally, this cloudy

Table 2: Hydrothermal process time, absorption wavelengths, band gap energy and nanoparticles size of prepared samples.

Sample code	hydrothermal process time (s) (±1)	Absorption edge wavelength (nm) (±1)	Band gap Energy (eV) (± 0.015)	Nanoparticles size (nm) (±0.01)
B4M3-1	440	280	4.429	2.03
B7M3-1	770	286	4.335	2.07
B12M3-1	1320	286	4.335	2.07
B17M3-1	1870	287	4.320	2.08
B22M3-1	2420	288	4.306	2.09
B32M3-1	3520	293	4.232	2.13

Table 3: Absorption edge wavelength, band gap energy and nanoparticle size of samples with different solution molarity.

Sample code	solution molarity (M) (±0.001)	Absorption edge wavelength (nm) (±1)	Band gap energy (eV) (± 0.015)	Nanoparticle size (nm) (±0.01)
B32M3-2	0.010	283	4.382	2.05
B32L3-2	0.050	294	4.218	2.14
B32H3-2	0.100	303	4.092	2.23

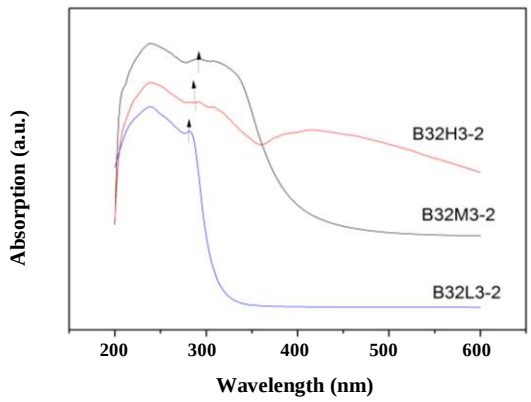

Fig. 4: Optical absorbance of samples with different solution molarity.

the net will be destroyed slowly by heating, and larger clusters will be formed, and for this reason, a red shift is expected.

The band gap energy of bulk SnO is about 2.5 eV, which is obviously smaller than the band gap energy of synthesized SnO nanoparticles. This difference in band gap energy can change the color of the material. When the band gap energy of a material increases, its absorption spectrum will shift to smaller wavelength; As a result, the color of the material will become lighter. Crystalline SnO is deep black while the prepared SnO nanoparticles were creamy white.

Fig. 4 shows optical absorbance of synthesized samples which were prepared by different solution molarities for the time 3520 s of microwave processing. The characterization of these samples is listed in Table 3. As shown in Fig. 4, other than the constant peak at 240 nm, there is a peak in wavelength of about 280 nm that has shifted to a higher wavelength by increasing the solution molarity. This red shift means that the size of nanoparticles increases by increasing solution molarity, and thus, the band gap energy decreases.

The optical absorption of samples with different pH is shown in Fig. 5. As shown in Fig. 5, the constant peak at 240 nm is still observed and there is also a peak at a wavelength of about 290 nm that has shifted to a higher wavelength by increasing final pH. The band gap energy and particle size were calculated from Equations (2) and (3) and listed in Table 4. Growth of the particles obviously occurred for the sample prepared at a pH = 9. It might have happened because this solution is in an alkaline environment and the particles tend to agglomerate and show bulky properties. Thus, it is concluded that an acidic environment prevents agglomeration and produces a smaller nanoparticle size.

To investigate the effect of microwave power, a sample was synthesized at the power of 500 W. The absorption spectrums and results are shown in Fig. 6 and Table 5. As can be seen, by increasing microwave power,

Table 4: Absorption edge wavelength, band gap energy and nanoparticle size of the samples synthesized by different final pH.

Sample code	Final pH (±0.01)	Absorption edge wavelength (nm) (±1)	Band gap energy (eV) (± 0.015)	Nanoparticle size (nm) (±0.01)
B32M3-1	1.00	291	4.261	2.12
B32M3-2.5	2.50	292	4.247	2.12
B32M3-3.5	3.50	294	4.218	2.14
B32M3-9	9.00	383	3.238	3.29

Table 5: Absorption edge wavelength, energy band gap and nanoparticle size of the samples synthesized by different microwave power.

Sample code	Microwave power (W)	Absorption edge wavelength (nm) (±1)	Band gap energy (eV) (± 0.015)	Nanoparticle size (nm) (±0.01)
B22M3-1	300	290	4.276	2.11
B22M5-1	500	292	4.247	2.12

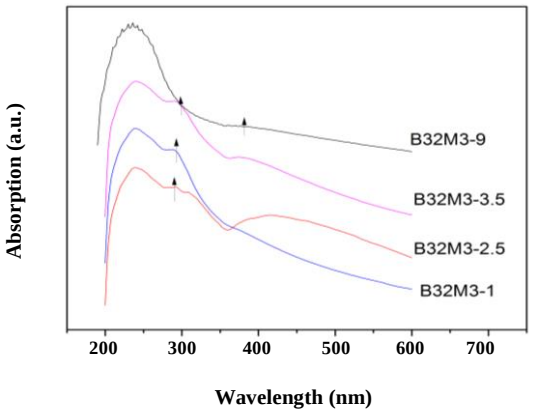

Fig. 5: Absorption spectrum for samples with different pH.

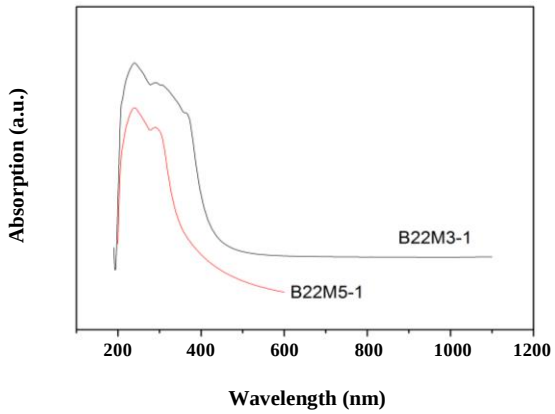

Fig. 6: Absorption spectrum of prepared samples by different microwave power.

the absorption wavelength has shifted to higher wavelengths that means increasing power leads to bigger particles. The SnO nanoparticles tend to oxidize and form tin(IV) oxide with a microwave power higher than 600 W.

Photoluminescence spectroscopy of sample B32M3-1 with an excitation wavelength at 240 nm and 290 nm was done and the spectra are shown in Fig. 7. There are two strong emission peaks at wavelength 394 and 454 nm with excitation wavelength at 240 nm and some shoulders at wavelengths 410, 429, 495 and 531 nm. In addition, there is a broad emission peak at wavelength 373 nm with excitation wavelength at 290 nm and some shoulders at wavelengths 419, 480 and 531 nm. The emission wavelengths are shown in Table 6.

Fig. 8 depicts the diagram of Ln (αhν) with respect to Ln (hν-Eg) for sample B32M3-2.5. As the results show, m is equal to 0.5, which indicates that SnO has a direct band gap equal to 2.5 eV.

To estimate the Urbach energy, the diagram of Ln α with respect to ħω for sample B32M3-2.5 is shown in Fig. 9.

As can be seen, the Urbach energy was estimated to be 2.7 eV by equation 6. The activation energy for prepared SnO nanoparticles was calculated to be 47.75 kJ/mol from equation 9.

CONCLUSIONS

Single phase SnO nanoparticles were synthesized using microwave radiation with different hydrothermal

Table 6: Emission wavelengths for different excitation wavelength of B32M3-1.

Excitation wavelength (nm) (±1)	Emission wavelength (nm) (±1)
240	394,410,429,454,495,531
290	373,419, 480,531

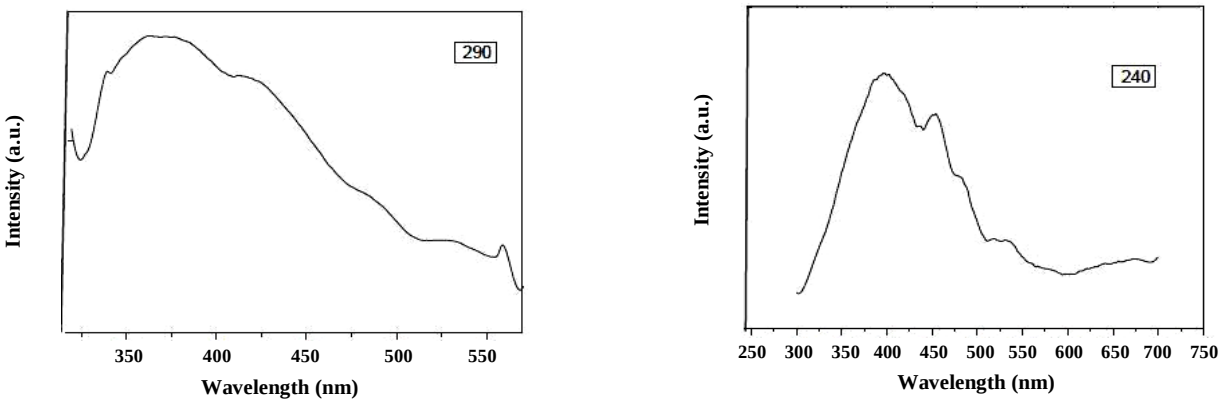

Fig. 7: Emission spectrum of B32M3-1 with excitation wavelength at a) 290 nm (left figure) and b) 240 nm (right figure)..

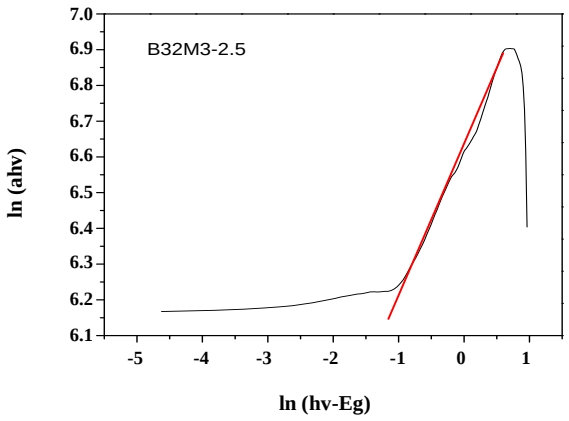

Fig. 8: The diagram of Ln (αhv) with respect to Ln (hv-E_g) for sample B32M3-2.5.

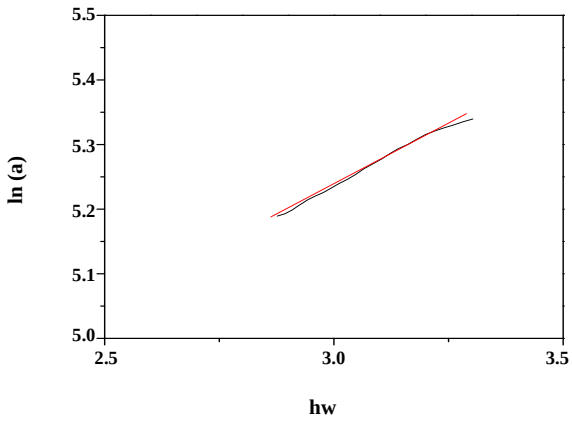

Fig. 9: The diagram Lnα with respect to ħω for sample B32M3-2.5, (y=0.37x + 4.13).

processing time, molarity, pH and radiation power, of the size of 2-5 nm have been obtained. The SnO samples show a strong excitonic peak in UV-Vis absorbance spectra about 280 nm which is absent in bulk SnO. This peak was shifted to higher wavelengths by increasing hydrothermal time process, solution molarity, microwave power, and final pH which resulted in bigger particle. In addition, it concluded that acidic environment prevents agglomeration and the solution in the acidic range produced smaller nanoparticle size. SnO nanoparticles also show strong peaks in the photoluminescence emission spectrum at wavelength 394 and 454 nm with excitation wavelength at 240 nm. From the aforementioned results, it can be concluded that the nanoparticles of tin(II) oxide have a direct band gap of about 2.5 eV. In addition, the activation energy and the Urbach energy were estimated to be 47.75 kJ/mol and 2.7 eV, respectively.

Received : May 24, 2017 ; Accepted : Dec. 4, 2017

REFERENCES

[1] Krishnakumar T., Jayaprakash R., Singh V.N., Mehta B.R., Phani A.R., Synthesis and Characterization of Tin Oxide Nanoparticle for Humidity Sensor Applications, *J. Nano Res.*, **4**: 91-101 (2008).

[2] Tomashyk V., "Quaternary Alloys Based on II - VI Semiconductors", CRC Press, (1993).

[3] Nwanya A.C., Ugwuoke P.E., Ezekoye B.A., Osuji R.U., Ezema F.I., Structural and Optical Properties of Chemical Bath Deposited Silver Oxide Thin Films: Role of Deposition Time, *Adv. Mater. Sci. Eng.*, **2013**: 450820 (2013).

[4] Peleckis G., "Studies on Diluted Oxide Magnetic Semiconductors for Spin Electronic Application", PhD Thesis, Institute of Superconductive and Electronic Material, University of Wollongong, (2006).

[5] Batzill M., Diebold U., The Surface and Materials of Tin Oxide, *Prog. Surf. Sci.*, **79**: 47-154 (2005).

[6] Vijayaprasath G., Ravi G., Hayakawa Y., Effect of Solvent on Size and Morphologies of SnO Nanoparticles via Chemical Co-precipitation Method, *Inter. J. Sci. Eng. Appl.*, Special Issue NCRTAM ISSN-**2319-7560** (Online): 21-23 (2013).

[7] Pires F.I., Joanni E., Savu R., Zaghete M.A., Longo E., Varela J.A., Microwave-Assisted Hydrothermal Synthesis of Nanocrystalline SnO Powders, *Mater. Lett.*, **62**: 239-242 (2008).

[8] Majumdar S., Chakraborty S., Devi P., Sen A., Room Temperature Synthesis of Nanocrystalline SnO through Sonochemical Route, *Mater. Lett.*, **62**: 1249-1251 (2008).

[9] Rellinghaus B., Linackers D., Kockerling M., Roth P., Wassermann E.F., The Process of Particle Formation in the Flame Synthesis of Tin Oxide Nanoparticle, *Phase Transitions*, **76**: 347-354 (2003).

[10] Jimenze V.M., Gonzalez A.R., Espinos J.P., Justo A., Fernandez A., Synthesis of SnO and SnO_2 Nanocrystalline Powders by the Gas Phase Condensation Method, *Sens. Actuators, B*, **31**: 29-32 (1996).

[11] Zheng H., Gu Ch.D., Wang X.L., Tu J.P., Fast Synthesis and Optical Property of SnO Nanoparticles from Choline Chloride-Based Ionic Liquid, *J. Nanopart. Res.*, **16**: 2288-2296 (2014).

[12] Um J., Roh B., Kim S., Kim S.E., Effect of Radio Frequency Power on the Properties of p-type SnO Deposited via Sputtering, *Mater. Sci. Semicond. Process.*, **16**: 1679-1683 (2013).

[13] Mote V.D., Purushotham Y., Dole B.N., Williamson-Hall Analysis in Estimation of Lattice Strain in Nanometer-Sized ZnO Particles, *J. Theor. Appl. Phys.*, **6**: 1-8 (2012).

[14] Svanberg S., "Atomic and Molecular Spectroscopy: Basic Aspects and Practical Applications", 4th ed., Springer, Germany (2004).

[15] Aydogu S., Sendil O., Coban M.B., The Optical and Structural Properties of ZnO Thin Films Deposited by the Spray Pyrolysis Technique, *Chin. J. Phys.*, **50**: 89-100 (2011).

[16] Kasap S., Capper P., "Springer Handbook of Electronic and Photonic Materials", Springer Science & Business Media (2007).

[17] Logan S.R., The Origin and Status of the Arrhenius Equation, *J. Chem. Educ.*, **59**: 279-283 (1982).

[18] Uysal B.O., Arier U.O.A., Structural and Optical Properties of SnO_2 Nanofilms by Spin-Coating Method, *Appl. Surf. Sci.*, **350**: 74–78 (2015).